Challenging Glass 5 – Conference on Architectural and Structural Applications of Glass
Belis, Bos & Louter (Eds.), Ghent University, June 2016.

ISBN 978-90-825-2680-6

Investigation of Bonded Connections with Silicone under Shear Loading

Y. Staudt [a], C. Odenbreit [a] & J. Schneider [b]
[a] *University of Luxembourg, ArcelorMittal Chair of Steel and Façade Engineering, Luxembourg, yves.staudt@uni.lu*
[b] *Technische Universität Darmstadt, Institute of Structural Mechanics and Design, Germany*

In façade applications, structural sealant glazing systems with a soft adhesive like silicones show a number of advantages especially regarding brittle adherends like glass sheets, as stress concentrations in the adherends are avoided due to the large bonding area and the uniform load transfer. The application guideline for structural sealant glazing systems (European Technical Application Guideline ETAG 002) defines a simplified design concept for the silicone sealant, leading to high safety factors and restrictions in use. The material behaviour of the silicone sealant can be more accurately described using the Finite Element Method and hyperelastic material laws, but the results for the stresses at the edge area for a shear dominated loading are highly mesh dependent, due to the presence of a singularity and thus hampering the assessment of the realistic stress distribution. In this paper, shear tests on bonded connections with silicone, referring to the ETAG 002, are presented. Beside the overlap length and adhesive thickness of the specimen prescribed by the standard, two more overlap lengths and thicknesses are tested. For the experimental investigations, the force-deformation behaviour and the failure initiation, observed at the edge area, are recorded. Unlike for the adhesive length, an influence of the specimen thickness on the failure shear strain could be observed and predicted by the numerical simulations. A clear difference between the maximum load and the load at failure initiation was observed.

Keywords: Structural sealant glazing system, Simple shear test, Stress peak, Failure

1. Introduction

1.1. Structural sealant glazing systems

In the context of innovative, energy efficient and architectural attractive façade systems, structurally bonded connections between the building's structure and the façade panels, as shown in figure 1, constitute an important joining technology. For the so-called structural sealant glazing systems, glass elements are adhesively bonded to the metallic substructure of the building, as shown in figure 2. For these connections, soft silicone sealants are generally used. The European Technical Application Guideline ETAG 002 (ETAG 002 2012), which is applicable for these kind of façade systems, even restricts the choice of the adhesive to silicones. This has several reasons. Silicone elastomers exhibit an excellent resistance against UV radiation and weather impact, showing almost constant properties over a wide temperature range. In addition, silicones are able to adhere on many materials, including glass, aluminium and steel (Habenicht 2009).

Fig. 1 Two sided structural sealant glazing system, Pollux and Castor towers in Frankfurt/Main, Germany (Dow Corning 2010)

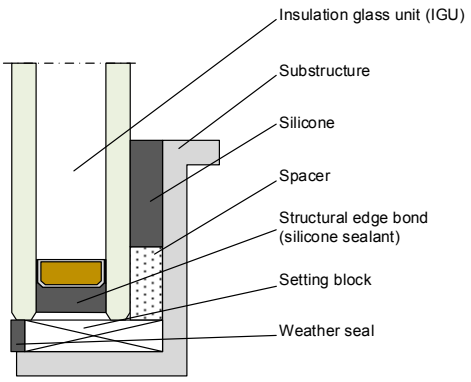

Fig. 2 Structural sealant glazing system – insulation glass unit adhesively bonded to the building substructure (ETAG 002 2012)

Regarding brittle materials like glass, bonded connections with a soft silicone adhesive allow to reduce stress concentrations in the adherends. The uniform transfer of loads due to the large bonding area, as well as the sealant's ability to compensate a differential thermal movement of the adherends avoid stress peaks, thus leading to a reduced thickness of the glass sheets (Staudt 2014).

1.2. Design of structurally bonded connections

For the design of structurally bonded connections, the ETAG 002 defines a number of requirements and restrictions. Furthermore, high design factors are prescribed, which is due to the current state of knowledge. In fact, the proposed design concept neglects many effects in the silicone sealant, assuming for example a uniform stress state in the adhesive (ETAG 002 2012). For the case of a bonded connection undergoing a differential thermal movement, as shown in figure 3, the stresses in the adhesive are evaluated as follows:

$$\tau = G \cdot \frac{\Delta L}{t} \leq \tau_{des} \tag{1}$$

Where τ is the acting shear stress, G the shear modulus of the sealant, ΔL the differential thermal movement, t the adhesive thickness and τ_{des} the design shear stress.

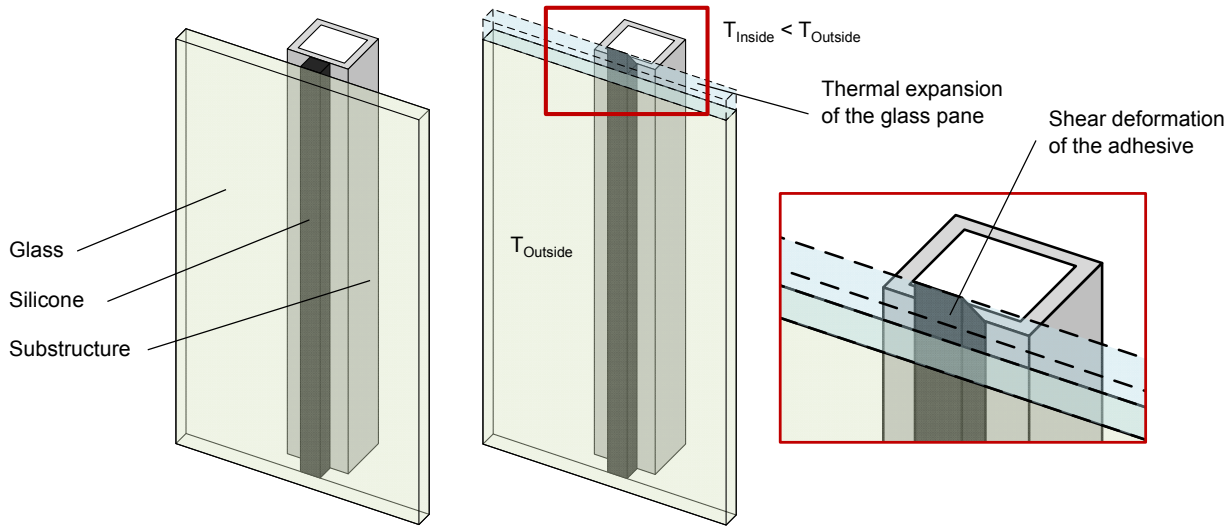

Fig. 3 Structurally bonded connection in a temperature load case, where the outside temperature $T_{Outside}$ is higher than the temperature inside the building T_{Inside}

1.3. Finite Element Analysis of the sealant

The previously described system can be numerically reproduced using the Finite Element Method, where the silicone elastomer is often modelled assuming incompressible hyperelastic material laws (Hagl 2007). For the simulation of the previously mentioned bonded connections subjected to a differential thermal movement, the stresses at the edge area of the bonded connection were found to be highly mesh dependent. This mesh dependency was already investigated in the works of (Dias 2013 and Staudt 2014).

The above mentioned mesh dependency is due to a singularity, which occurs at the corner edge of the interface between the adhesive and the adherend. This singularity leads to increasing values of the stresses and strains at the corner edge for a refined mesh, as the integration points move closer to the origin of the singularity, when smaller elements or elements with higher order are used (Weißgraeber 2013).

The mesh dependency is visualised in figure 6, where the shear stresses are plotted over a horizontal path for the specimen detailed in the ETAG 002, shown in figure 4, and the boundary conditions given in figure 5. A nonlinear 3D finite element analysis with the model characteristics detailed in the third section was carried out using the commercial finite element software code ABAQUS®. Two paths were chosen, one at the centreline of the adhesive and one at the interface between the adhesive and the adherend. Whereas the stresses at the centreline of the adhesive give a constant value for all the considered meshes, the stresses at the corner point of the interface between the adhesive and the adherend show a peak with increasing values for a refined mesh.

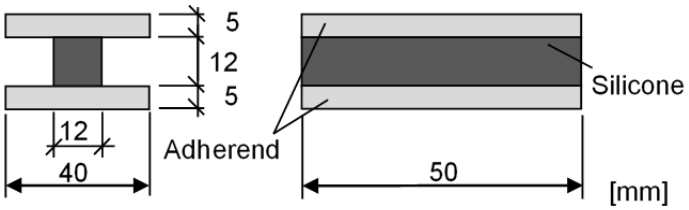

Fig. 4 ETAG 002 specimen

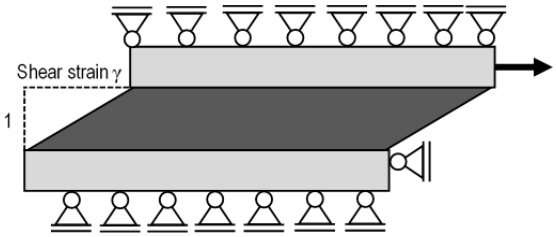

Fig. 5 Supposed boundary conditions

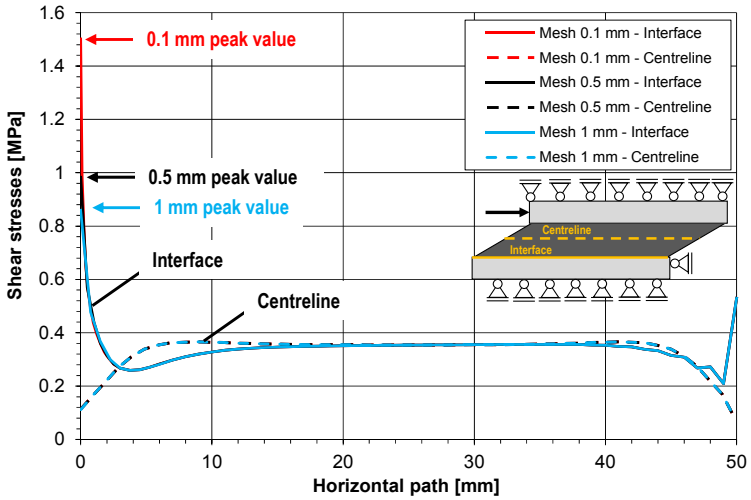

Fig. 6 Mesh study on the shear stress distributions for a path at the centreline and a path at the interface between the adhesive and the adherend

1.4. Methodology and objectives

It has been mentioned previously that the results of the finite element analysis are highly mesh dependent due to the singularity at the bi-material interface, thus not allowing for an accurate assessment of the stress state close to the corner edge. In order to investigate the influence of the corner stresses on the load bearing capacity, shear tests were conducted. The accuracy of the numerical simulation was evaluated and the load bearing capacity of bonded connections in shear quantified with regard to different parameters of influence. Simple failure criteria are evaluated using the experimental data.

2. Experimental investigations

2.1. Objectives

The objective of the presented experimental investigations is the determination of the force-deformation behaviour in shear and the failure load for bonded connections with Dow Corning 993® structural silicone sealant. The specimen detailed in the ETAG 002 was used and modified for the presented shear tests.

2.2. Specimen and investigated parameters

For the conducted shear tests, specimen analogous to ETAG 002 were chosen. In distinction from the requirements in the ETAG 002, steel was used as adherends in order to compare the results with previously conducted tests described in (Dias 2013). For one test series, aluminium adherends were used in addition in order to investigate the influence of the adherends' material on the test results.

The standard specimen foreseen by the ETAG 002 with a length of 50 mm and a thickness of 12 mm is shown in figure 4. Apart from this, specimen with half and double thickness (i.e. 6 mm and 24 mm) as well as specimen with a length of 100 mm and 200 mm were tested in addition to the standard specimen. The definition of the thickness and the length of a specimen is given in figure 7.

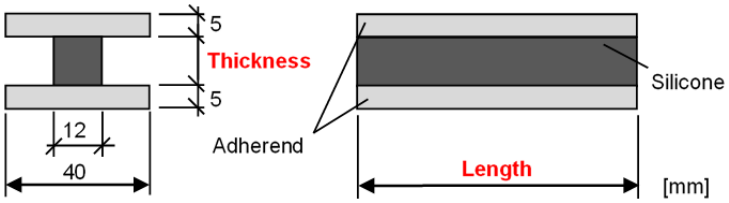

Fig. 7 Specimen used for the shear tests – definition of the thickness and the length

The specimen were loaded in displacement control, i.e. a constantly increasing shear displacement was applied on the specimen according to figure 5. For one test series, some specimen were loaded with a constantly increasing shear force. Table 1 summarises the chosen parameter of influence in a test matrix.

Table 1: Investigated parameters, designation and number of specimen

Thickness t [mm]	Length l [mm]		
	50	100	200
6	50-6: 5	100-6: 5	-
12	50-12: 5 50-12-ALU: 5 (aluminium adherends)	100-12: 6 100-12-LOAD: 3 (force applied)	200-12: 5
24	-	100-24: 5	200-24: 5

For the production of the specimen, the adherends were carefully cleaned using an appropriated solvent (Dow Corning® R40) and a primer (Dow Corning® 1200 OS) was applied prior to the pouring of the silicone. The adherends were separated using a mould of polyethylene material as illustrated in figure 8. The adherends and the mould were fixed together with either screws or screw clamps. The two components of the silicone sealant were mixed with a two component mixing plant. After the pouring of the silicone, the specimen were stored for 4 weeks at ambient temperature and humditiy.

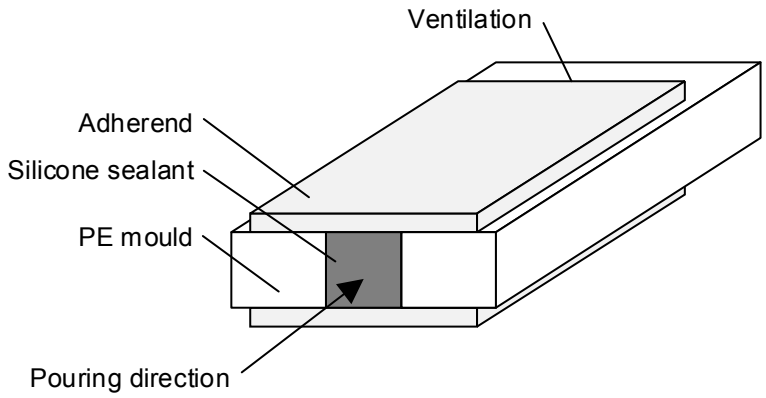

Fig. 8 Production of the specimen using a polyethylene mould

2.3. Test setup

The test setup is shown in figure 9 and figure 10. It is basically composed of two parallel plates, where the left plate is fixed to the 10 kN Instron hydraulic jack used and the right plate to the cross beam of the testing frame.

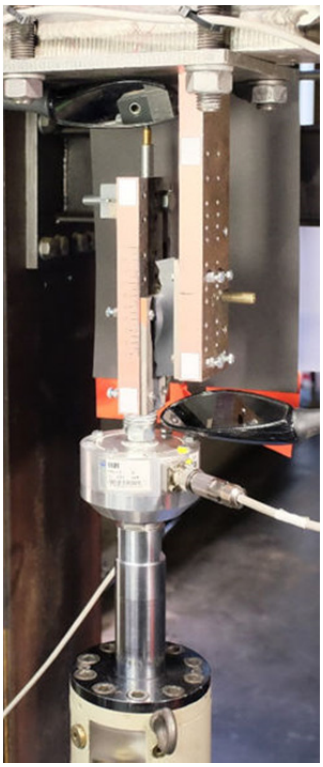

Fig. 9 Test setup at the ArcelorMittal Chair of Steel and Façade Engineering

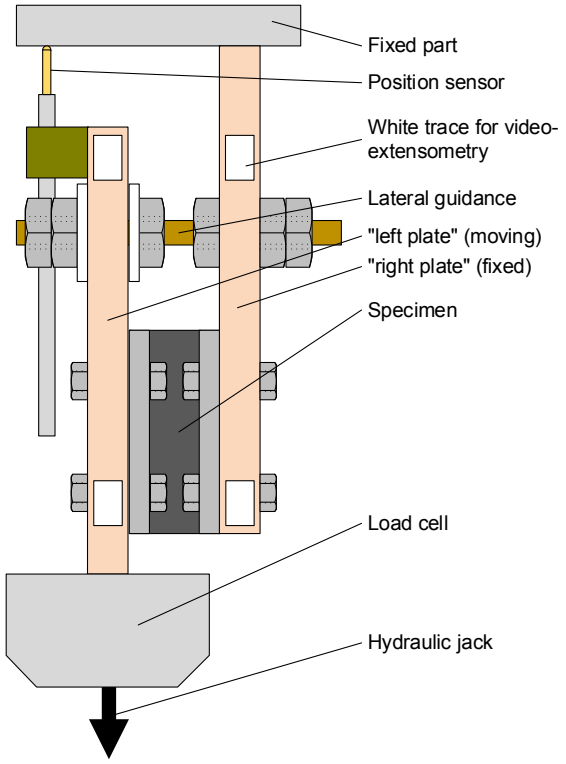

Fig. 10 Schematic sketch of the test setup

As horizontal forces due to the peel stresses occur in this kind of simple shear tests, a lateral guidance consisting of a threaded rod was used. The right plate was equipped with a threaded hole and the left one with a slot. Nuts were placed at both sides of the moving plate. In order to avoid friction, washers made out of PTFE were used in combination with grease. Before and after each test series, the friction of the test setup was evaluated by running an empty test, i.e. without specimen. A friction force less than 10 N was recorded, even when applying a horizontal force on the left plate.

Concerning the measurement equipment, a 5 kN load cell was added between the hydraulik jack and the left plate. In addition, an inductive position sensor was used to record the relative displacement between the two plates. The horizontal displacement between the steel plates was checked using video-extensometry. It was found that the relative horizontal displacement between the two plates was smaller than 0.1 mm. The recorded video was furthermore used to observe the failure process of the specimen.

The specimen used were fixed on the plates using screws and nuts in order to guarantee a parallel displacement between the two adherends, as assumed in the boundary conditions in figure 5. The tests were carried out at ambient temperature. The loading rate was determined applying the principle of constant energy input described in (Scherer 2014). According to this, the shear displacement velocity can be determined as follows:

$$\dot{\gamma} = \frac{d\gamma}{dt} = \frac{1}{h} \cdot \frac{du}{dt} = \frac{1}{h} \cdot \dot{u} = const. \tag{2}$$

Where γ is the engineering shear strain, t the testing time, u the imposed displacement and h the thickness of the specimen. The constant value is calculated from the imposed energy input at the uniaxial tensile tests. Taking into consideration the tensile tests at low velocity described in (Staudt 2014), a value of 1 mm/min was found for the 6 mm thickness specimen of the shear tests. According to equation (2), 2 mm/min are obtained for the 12 mm specimen and 4 mm/min for the 24 mm specimen.

2.4. Results

The results of the shear tests are shown in figure 11. An average curve is shown for each test series. The number of specimen for each series is given in table 1. The scattering of the results is in the order of magnitude of 5-10%. The recorded forces were divided by the product of bite and length to obtain an engineering or averaged shear stress and the recorded displacements by the thickness of the specimen in order to get an engineering shear strain. The engineering stress-strain curves in figure 11 are plotted until the average failure strain and failure stress observed for

the respective series. Failure was defined as the appearance and opening of a significant crack, which can be captured as an offset or a change of the slope of the force-deformation curve.

The results in figure 11 show that the stress-strain relationship is independent of the chosen length and thickness of the specimen as the curves are coincident. A clear nonlinear behaviour can be observed in the range of small deformations. For large deformations, the curves follow a straight line.

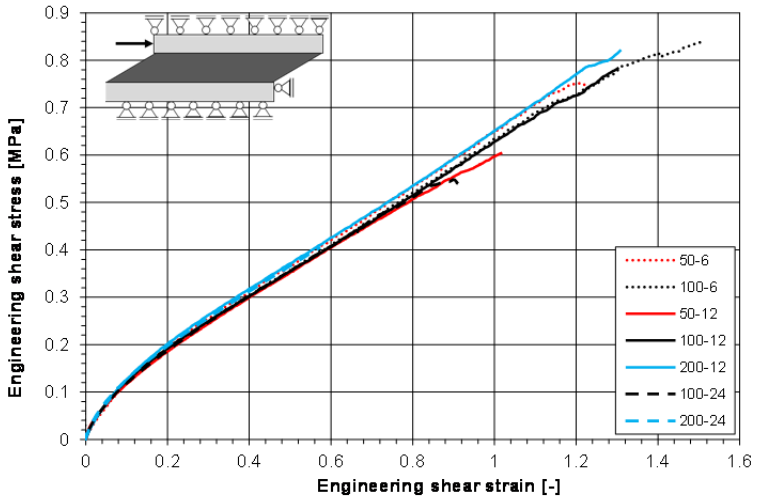

Fig. 11 Results of the shear tests – engineering shear stresses and shear strains are shown. One average curve is plotted per test series up to the average failure point for the respective series.

Apart from the defined failure point, the maximum recorded load was evaluated as well. Figure 12 shows the results of failure engineering stresses and strains for the different test series (average value and standard deviation are given). For each test series, the results for failure initiation (engineering shear stress and strain) and the results for the maximum load level (engineering shear stress) are given.

In figure 12, it can be observed that the average engineering stress at maximum load is about 5-25% higher than the average engineering stress at failure. Moreover, no significant difference is found between the steel and aluminium adherends. For the specimen loaded with a constantly increasing force, again no significant difference compared to the specimen tested in displacement control was observed. The influence of the adhesive thickness and length is discussed in section 4.

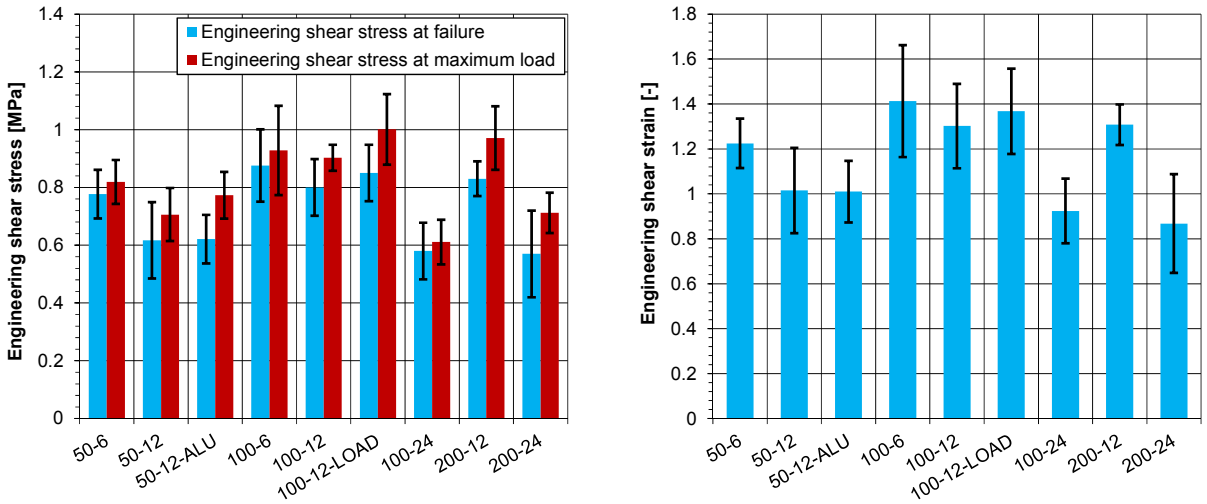

a) Engineering shear stress

b) Engineering shear strain at failure

Fig. 12 Engineering shear stresses and strains for the failure point (appearance of a significant crack) and engineering shear stresses at the maximum load level. The average value and the standard deviation are given for each series.

2.5. Analysis of the failure process of a typical specimen

In the present section, the failure process of two typical specimen is analysed. Figure 13 shows the stress-strain relationship for the specimen 100-24-05 and the average curve for that series. Moreover, 5 points are selected with the corresponding video frames shown in figure 14 a) to e). For point a), no failure is observed, whereas in point b), an offset in the stress-strain curve was recorded. Figure 14 b) clearly shows a crack opening at the corner edge of the bonded connection. After this offset in the engineering stress-strain curve, the transferred load still increased, as can be seen at point c), where the crack has grown compared to point b). At point d), a second crack at the opposite corner edge has appeared and the stress-strain curve was finally decreasing. At the final point e), the crack has significantly grown and the load significantly decreased.

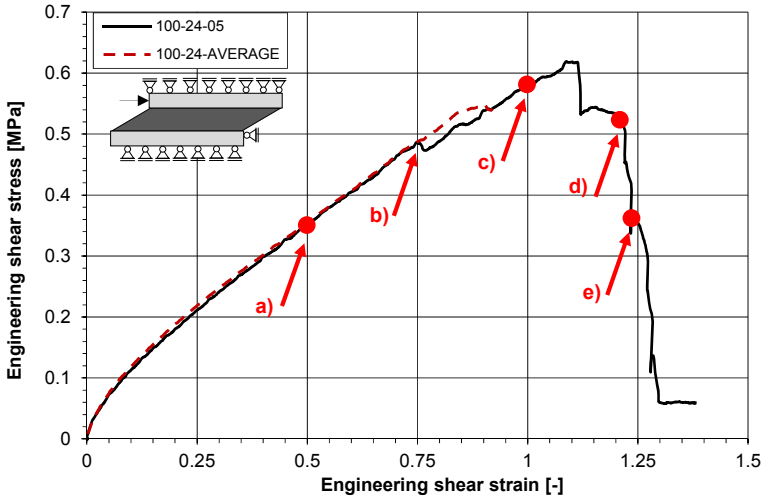

Fig. 13 Engineering stress-strain curve in shear for the 100-24-05 specimen and average curve for the test series 100-24 plotted.

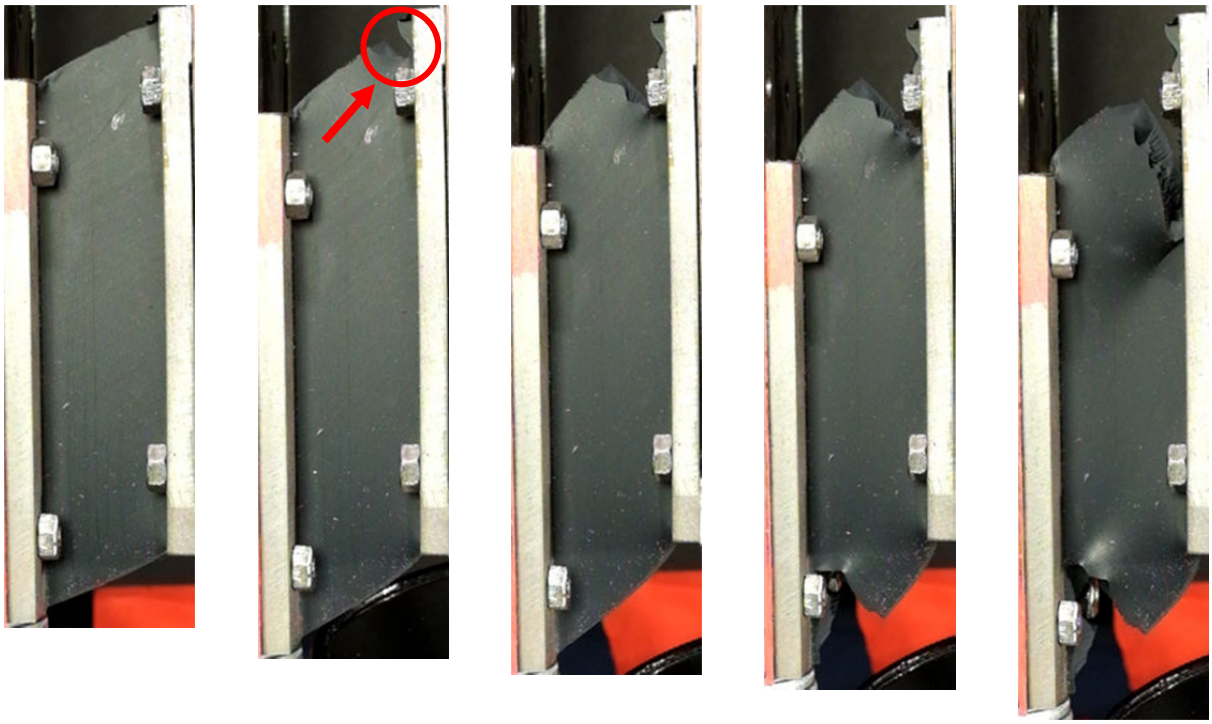

a) $\gamma = 0.50$ b) $\gamma = 0.75$ c) $\gamma = 1.00$ d) $\gamma = 1.13$ e) $\gamma = 1.21$

Fig. 14 Observed deformations for the points given in figure 13. γ is the engineering shear strain.

In the second example, a specimen is shown, for which a first crack was already discovered at very low displacements, as shown in figure 16 b). The actual failure of this specimen however was identified at the point of the stress-strain diagram in figure 15, where the slope of the curve has changed, as indicated in point c) with the dotted line.

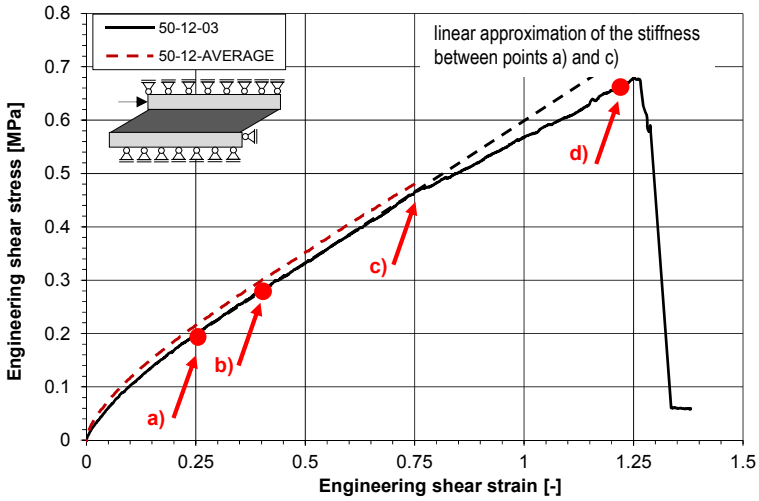

Fig. 15 Engineering stress-strain curve in shear for the 50-12-03 specimen and average curve for the test series 50-12 plotted.

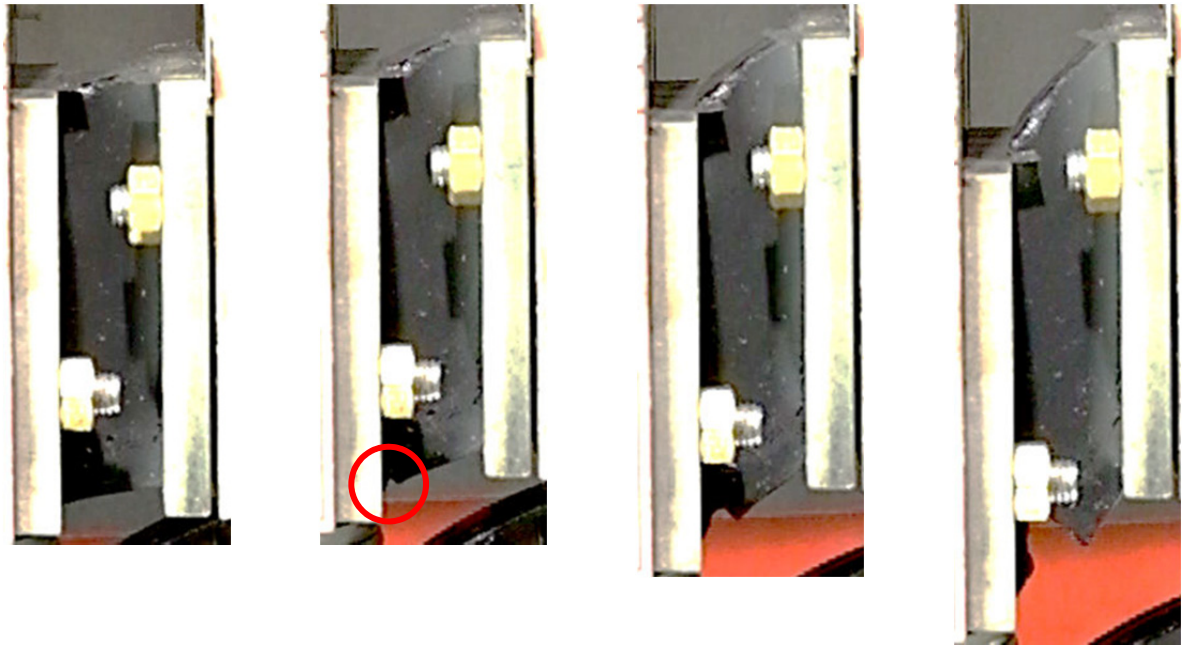

a) $\gamma = 0.25$ b) $\gamma = 0.40$ c) $\gamma = 0.75$ d) $\gamma = 1.20$

Fig. 16 Observed deformations for the points given in figure 15. γ is the engineering shear strain.

2.6. Discussion of the results

The test results have shown the clear nonlinear behaviour of the silicone sealant. The stress-strain curves for all test series, i.e. for the considered lengths and thicknesses, are coincident. After a nonlinear increase for small strains, the curves follow a straight line up to the previously defined failure point. Failure however does not occur at the same stress or strain level for the different test series, as can be seen in figure 12.

A clear difference between the defined failure point of the specimen and the maximum load level could be observed, as discussed in the previous section. As the tests were conducted in displacement control, in the following section, the behaviour of the silicone sealant under a constantly increasing force was investigated.

2.7. Analysis of the load bearing capacity after crack initiation

Three specimen of the test series 100-12 were chosen and loaded with a constant loading rate of 2 N/s. This loading rate corresponds to an average loading rate observed in the displacement controlled tests. For the specimen 100-12-08, the load was constantly increased until complete failure of the specimen. For the two other specimen, the load was held constant for 20 minutes after crack initiation. The engineering stress-strain curves for the three specimen are shown in figure 17. The non-linear material behaviour can again be clearly observed.

In figure 18, the applied force against the testing time is plotted. For the 100-12-09 specimen, the load was increased to 900 N. As no failure was observed, the load was further increased to 1000 N. At this level, failure was observed (red arrow in figure 18) and the load was held constant during 20 minutes. Hereafter, the load could be further increased in steps of 100 N up to the maximum load level. Between each load increase, the force was held constant for 60 s.

Similar behaviour was observed for the 100-12-10 specimen. For this specimen, failure occurred at 900 N. Again, the load was held constant for 20 minutes before increasing the load to the maximum load level.

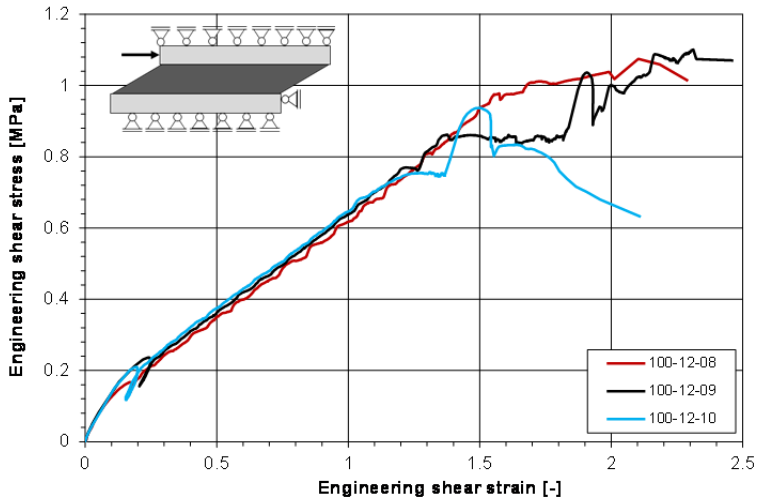

Fig. 17 Stress-strain (engineering values) behaviour in shear for the specimen of the test series 100-12-LOAD.

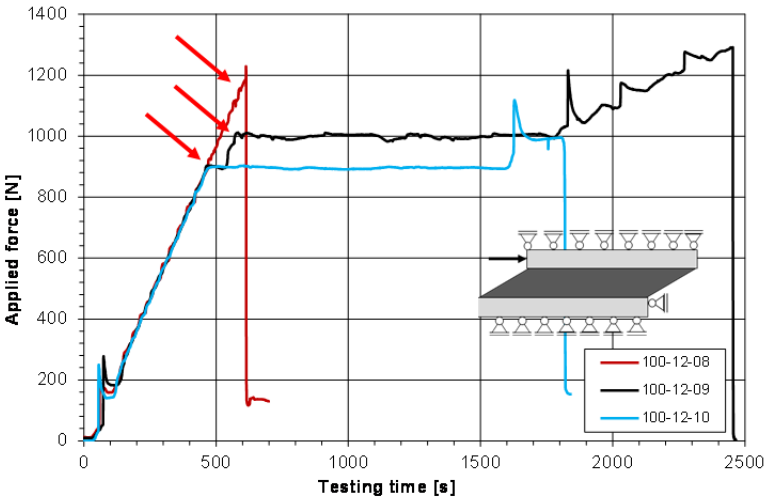

Fig. 18 Applied force plotted against testing time for the series 100-12-LOAD. The arrows are indicting the failure point of the specimen.

3. Numerical simulation

3.1. Hyperelastic material law

For the numerical simulation of the silicone elastomer, the hyperelastic *Marlow* model was used. The *Marlow* model is available in the commercial finite element software code ABAQUS®. The *Marlow* model assumes that the strain energy density only depends on the first invariant of the left *Cauchy-Green* deformation tensor. For this reason, the material response can be directly determined from test data without need for an explicitly given function for the strain energy density (Marlow 2003).

For the numerical reproduction of the shear tests, the uniaxial tensile test data presented in (Staudt 2014) was used for the characterisation of the *Marlow* model. An incompressible material behaviour was assumed for the silicone sealant as the bulk modulus is much higher (factor 600) than the shear modulus (Dias 2013).

3.2. Numerical model and boundary conditions

The shear test was numerically reproduced using the commercial finite element software code ABAQUS®. 20-node quadratic fully integrated brick elements with hybrid formulation due to the incompressible material behaviour of the adhesive were chosen in the geometrical non-linear analysis. The assumed boundary conditions are visualised in figure 19. A mesh size of 1 mm, giving convergent results regarding the force-deformation behaviour, was used in the analysis and symmetry in bite direction was assumed. The adherends were not modelled in the analysis since they are rigid compared to the soft silicone sealant.

Fig. 19 Applied boundary conditions for the numerical model. Only the silicone sealant is modelled due to the high rigidity of the adherends compared to the sealant.

3.3. Results

Figure 20, 21 and 22 show the results of the finite element analysis. A very good agreement between the experimental data and the numerical simulation is found for all the test series. Again, the force-deformation results from the finite element analysis were transformed into engineering stress and strains values according to the previously mentioned procedure.

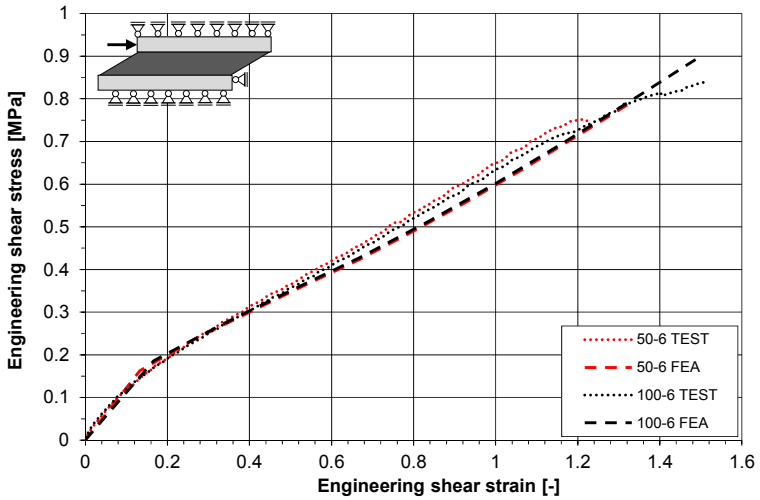

Fig. 20 Experimental and numerical results of the engineering stress-strain curve in shear for the specimen of 6 mm thickness.

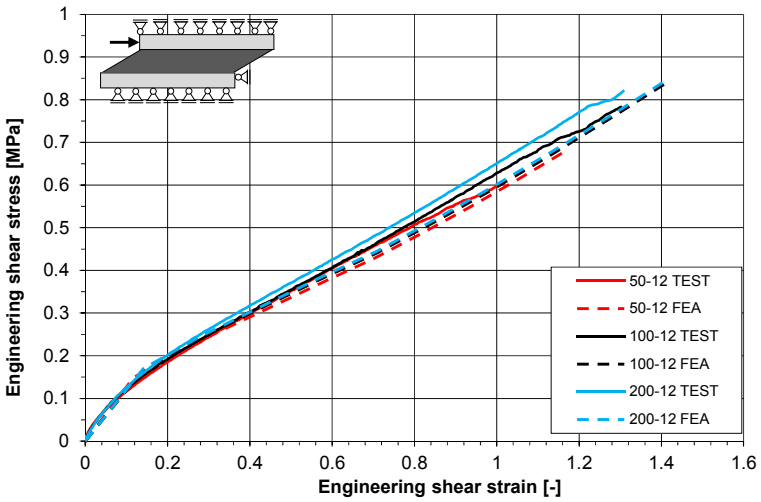

Fig. 21 Experimental and numerical results of the engineering stress-strain curve in shear for the specimen of 12 mm thickness.

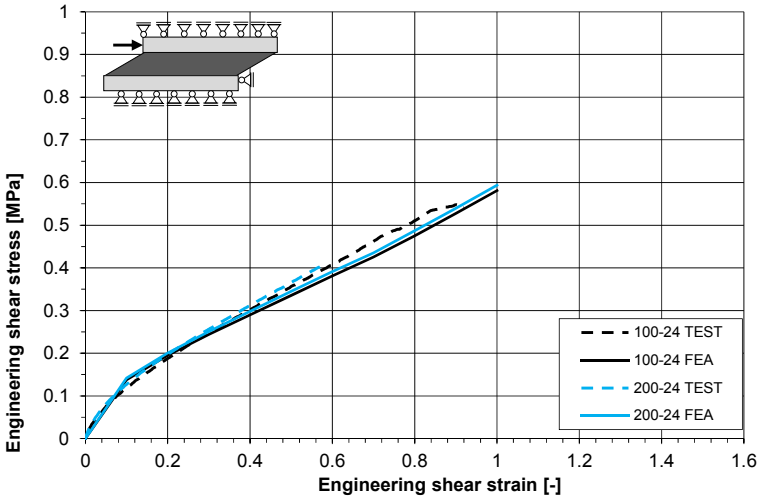

Fig. 22 Experimental and numerical results of the engineering stress-strain curve in shear for the specimen of 24 mm thickness.

Concluding, the chosen *Marlow* model with the assumption of incompressible material behaviour gives a good reproduction of the experimental curves. Failure however is not covered by this analysis.

3.4. Stress calculation

In the current section, the stress distribution obtained by a finite element analysis of the silicone sealant is considered in more detail. The boundary conditions of the model are given in section 3.2. In figure 23, the shear stress distribution is plotted for a horizontal path at the interface between adhesive and adherend. The stress distribution is evaluated for the considered lengths of the sealant and a constant thickness of 12 mm. For the three cases, a horizontal displacement of 12 mm was applied on the upper adherend and the same element size of 1 mm was chosen for all three simulations. The stress distributions for the different lengths are coincident at the edge area, as shown in figure 23. After this stress peak, an almost constant value is obtained.

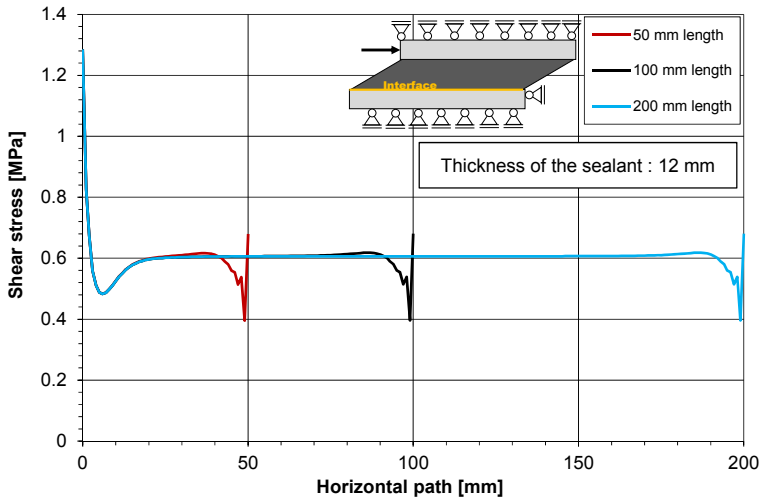

Fig. 23 Shear stress distribution in the silicone sealant at the interface to the adherend for different lengths and the same element size as well as the same applied displacement. A constant thickness of 12 mm is considered for the sealant.

The same procedure was carried out for the specimen with a length of 100 mm and the three different thicknesses (6 mm, 12 mm and 24 mm). Figure 24 shows the stress distribution in the silicone sealant at the interface between silicone and steel for the three considered thicknesses. Again, the finite element model detailed in section 3.2 was used and a constant engineering shear strain of 1 (i.e. a displacement of 6 mm for the specimen with a thickness of 6 mm for example) was applied for the considered specimen. Again, the same element size of 1 mm was used for the three models for a simplified comparison of the stress levels using identical meshes. In figure 24, it can be observed that the shear stresses at the edge area increase with the thickness. So, for the same applied shear strain, the 24 mm specimen exhibits the highest peak value. Figure 25 shows the stress distribution in the centreline of the adhesive for the same model as described before. At the centreline, the shear stress distribution is almost constant, with the highest value obtained for the specimen with a thickness of 6 mm.

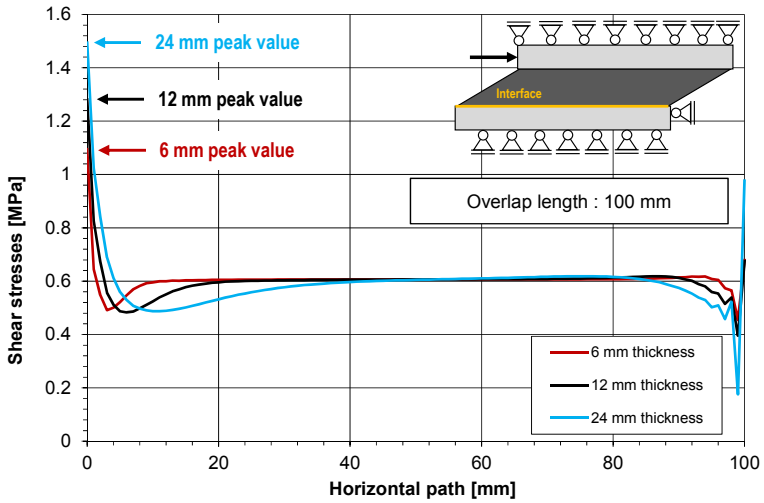

Fig. 24 Shear stress distribution in the silicone sealant at the interface to the adherend for different thicknesses and the same element size as well as the same applied engineering shear strain. A constant overlap length of 100 mm is considered.

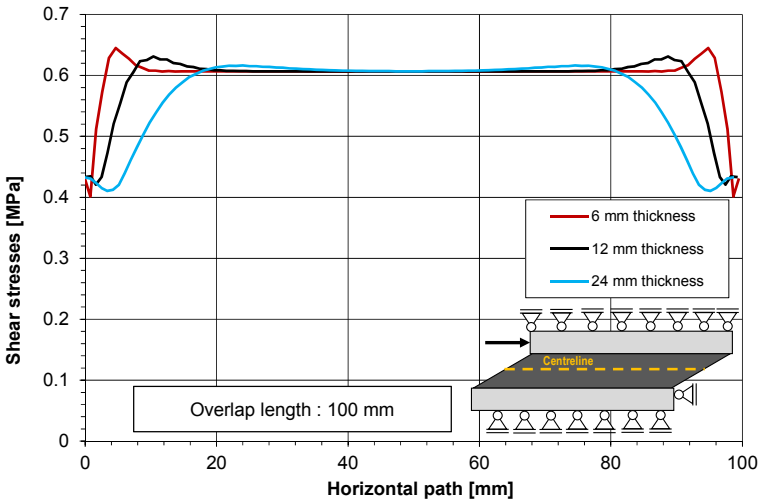

Fig. 25 Shear stress distribution at the centreline of the silicone sealant for different thicknesses and the same element size as well as the same applied engineering shear strain. A constant overlap length of 100 mm is considered.

4. Failure analysis

Concerning the failure of the specimen, the two main parameters investigated were the thickness and the length of the specimen. The engineering shear stress and the engineering shear strain were used to describe failure of the specimen. Shear stresses and shear strains at the failure point are proportional with a factor of 0.63 MPa, which corresponds to the shear modulus of Dow Corning 993®.

Figure 26 shows the recorded average engineering shear strains at failure plotted against the specimen thickness. The error bars are indicating the standard deviation of the considered test series. The number of specimen of each test series is given in table 1. It was found that the shear strain at failure decreases with increasing thickness. This is in accordance with the finite element calculation, which shows for the same mesh size a higher stress level for the thicker specimen at the corner edge of the interface, whereas the centreline values give the constant stress value for the same imposed engineering shear strain.

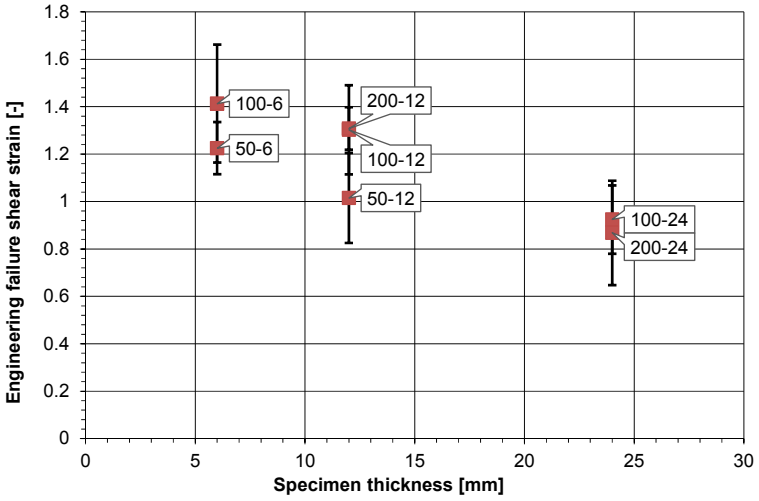

Fig. 26 Engineering strains at failure plotted against the thichness of the specimen. The error bars indicate the standard deviation for each test series.

Figure 27 shows the influence of the specimen length to failure. No clear trend can be observed. For each length however, the failure stresses are higher for the specimen with lower thickness, which has already been discussed in the previous paragraph.

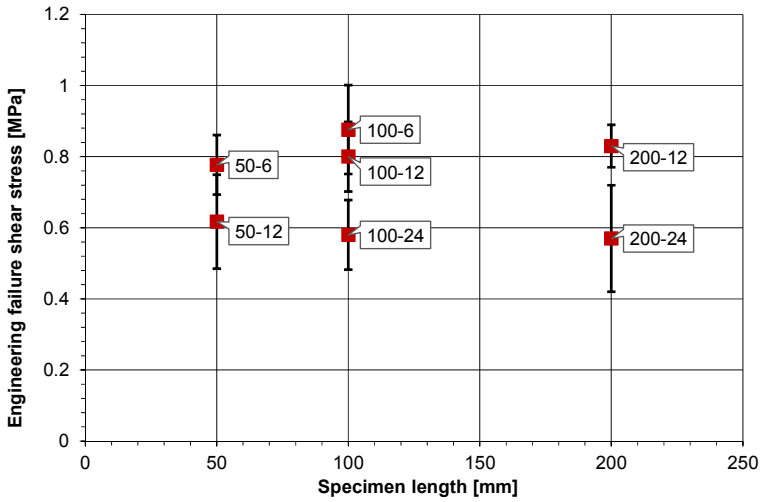

Fig. 27 Engineering stresses at failure plotted against the length of the specimen. The error bars indicate the standard deviation for each test series.

The trends observed in figure 26 and figure 27 were numerically predicted. Regarding the influence of the specimen thickness, the stresses were higher for a thicker silicone bead and the same applied engineering shear strain. This trend is found in figure 26, where the failure strain decreases for an increased thickness of the silicone. Concerning the length of the specimen, no clear trend was found in figure 27, which correlates with the fact that the stress plots are coincident for a constant thickness and the same engineering shear strain applied.

5. Conclusions and Outlook

Shear tests referring to ETAG 002 (ETAG 002 2012) with several lengths and thicknesses were carried out and numerically reproduced. Very good agreement was found for the reproduction of the stress-strain behaviour. Concerning the failure, the thickness of the specimen has an influence on the failure stress or strain. This trend can be confirmed by the numerical simulations considering the stress distribution at the interface of the adhesive. In a next step, a model should be elaborated to describe the failure in more detail.

In the experimental investigations, failure was defined when an offset or a change of the slope of the stress-strain curve occurs. In the tests, an increase of the applied load was observed even after the appearance of an initial crack. The failure process should be considered in more detail in future investigations.

Acknowledgements

The Hunsrücker Glasveredelung Wagener GmbH & Co. KG from Kirchberg (Hunsrück, Germany) is gratefully acknowledged for the pouring of the silicone sealant.

References

Dias, V. Development of adhesives constitutive material laws for the assessment of bonded steel to glass partial composite beams. PhD-thesis. University of Luxembourg, 2013.

Dow Corning Corporation: Case study – Forum Hochhaus Frankfurt am Main, Germany. Form number 62-1298C-01 (2010).

ETAG 002. Guideline for European Technical Approval for Structural Sealant Glazing Kits. European Organisation for Technical Approvals, 2012

Habenicht, G.: Kleben - Grundlagen, Technologien, Anwendungen. Vol. 6. Berlin, Heidelberg: Springer, 2009

Hagl, A.: Bemessung von strukturellen Silikon-Klebungen. Stahlbau 76, Heft 8, 569-581 (2007).

Marlow, R.S.: A general first-invariant hyperelastic constitutive model. In: Busfield & Muhr (eds.) Constitutive Models for Rubber III, pp. 157-160. Swets & Zeitlinger, Lisse (2003).

Scherer, T. Werkstoffspezifisches Spannungs-Dehnungs-Verhalten und Grenzen der Beanspruchbarkeit elastischer Klebungen. Dissertation Technische Universität Kaiserslautern, Germany, 2014.

Staudt, Y., Schneider, J., Odenbreit C. Investigation of the material behaviour of bonded connection with silicone. Engineered transparency international conference at glasstec. Düsseldorf, Germany, 2014.

Weißgraeber, P., Becker, W. Finite Fracture Mechanics model for mixed mode fracture in adhesive joints. International Journal of Solids and Structures, 50, pp. 2383-2394, 2013.